Modeling Action Potential Propagation in Unmyelinated Axons

Bachelor's Thesis

Student:	Raigo Milvaste
Student ID:	222390YAFB
Supervisors:	Researchers Kert Tamm, Tanel Peets
Curriculum:	Applied Physics

Tallinn, 2025

Aktsioonipotentsiaali leviku modelleerimine müeliniseerimata aksonites

Bakalaureusetöö

Student:	Raigo Milvaste
Student ID:	222390YAFB
Supervisors:	Teadlased Kert Tamm, Tanel Peets
Curriculum:	Rakendusfüüsika

Tallinn, 2025

Author Declaration

I hereby confirm that I have written this bachelor's thesis independently and that it has not been previously submitted for defense by anyone else. All the works of other authors, important viewpoints, and data originating from literature or elsewhere used in this thesis are properly referenced.

Author: Raigo Milvaste

This thesis meets the requirements for a bachelor's thesis.

Supervisors: Kert Tamm, Tanel Peets

Tallinn, 2025

Contents

Abstract

This thesis presents a version of the Hodgkin-Huxley (HH) model, called here the Lieberstein-modified HH model, which is used to simulate action potentials (APs) propagation in unmyelinated axons. We use a numerical method that relies on Fourier transforms for space and a Runge-Kutta method for time evolution. We demonstrate how APs form and travel under different conditions, such as by varying the stimulus strength or timing changes, and how some of the neuron's properties affect the AP signal transmission.

Abstract

See lõputöö esitab versiooni Hodgkin-Huxley (HH) mudelist, mida siin nimetatakse Liebersteini modifitseeritud HH mudeliks, mida kasutatakse aktsioonipotentsiaalide (AP) leviku simuleerimiseks müeliniseerimata aksonites. Kasutame numbrilist meetodit, mis tugineb ruumi jaoks Fourier' teisendustele ja aja evolutsiooni jaoks Runge-Kutta meetodile. Näitame, kuidas AP-d moodustuvad ja liiguvad erinevates tingimustes, näiteks muutes stiimuli tugevust või ajastuse muutusi, ja kuidas mõned neuroni omadused mõjutavad AP-signaali edastamist.

1 Introduction

Neurons transmit information through electrical impulses known as action potentials (APs), which are rapid, transient changes in membrane potential that propagate along the axon [7]. These signals are typically initiated at the axon hillock, following the integration of synaptic inputs received at the dendrites and soma (cell body) (see Fig. 1). Once triggered, the action potential travels along the axon to the synaptic terminals, where it induces the release of neurotransmitters into the synaptic cleft (see Fig. 2). These chemical messengers then bind to receptors on the dendrites of a subsequent neuron, facilitating the continuation of the signal. The biophysical basis of action potential generation was described by Hodgkin and Huxley [1], who demonstrated how voltage-dependent sodium and potassium ion channels underlie this process.

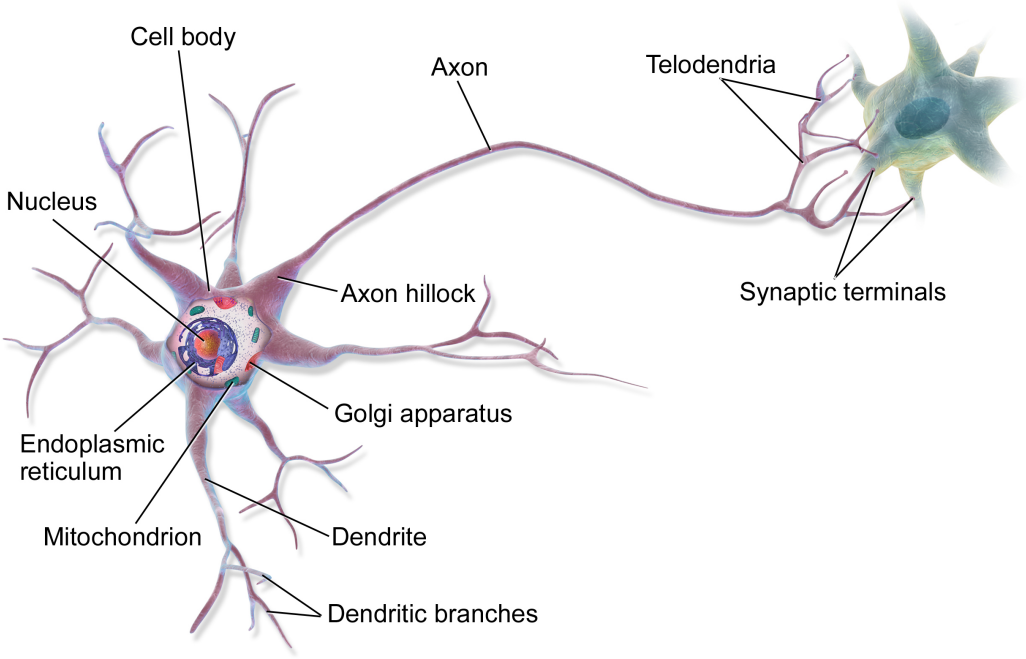

Figure 1: An axon of a multipolar neuron [12]

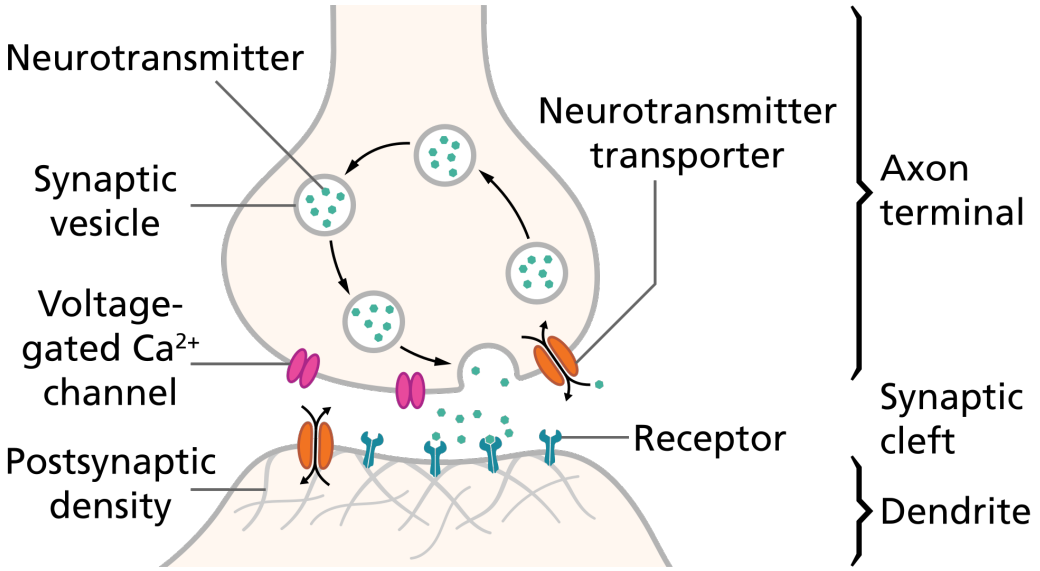

Figure 2: Neurotransmitter released from presynaptic axon terminal, and transported across synaptic cleft to receptors on postsynaptic neuron [11]

The original Hodgkin-Huxley (HH) model simplifies the axon by treating it as a resistor-capacitor circuit and does not include inductive effects. This makes the equations easier to solve, but limits how well they describe signal speed and shape, especially in long axons. In 1967, Lieberstein suggested a model that adds inductance and internal capacitance to the system [2]. This results in a set of equations that describe wavelike behavior.

In this thesis, we implement a version of Lieberstein's model and simulate AP propagation in unmyelinated axons. We apply a Fourier pseudospectral method to approximate spatial deriviates and use a Runge-Kutta method integration in time. Our simulations test how APs form and travel under different conditions, such as by varying the axon's electrical properties or geometry.

Abbreviations

Abbreviation	Full Term
AP	Action Potential
HH	Hodgkin-Huxley
AIS	Axon Initial Segment
ODE	Ordinary Differential Equation
PDE	Partial Differential Equation
FFT	Fast Fourier Transform
DFT	Discrete Fourier Transform
RLC	Resistor–Inductor–Capacitor (circuit)
Cm	Membrane Capacitance per unit area [μF/cm^2]
Ca	Axoplasmic Capacitance per unit volume [μF/cm^3]
R	Axial Resistance [Ω·cm]
Ra	Axial Resistance per unit length [Ω/cm]
L	Inductance per unit length [mH·cm]
g_K	Potassium Channel Conductance [m.mho/cm^2]
g_{Na}	Sodium Channel Conductance [m.mho/cm^2]
g_L	Leak Channel Conductance [m.mho/cm^2]
V_K	Potassium Reversal Potential [mV]
V_{Na}	Sodium Reversal Potential [mV]
V_L	Leak Reversal Potential [mV]
α_n, β_n	Rate constants for potassium activation gate
α_m, β_m	Rate constants for sodium activation gate
α_h, β_h	Rate constants for sodium inactivation gate
n, m, h	HH gating variables
RK	Runge-Kutta (numerical integration method)

Table 1: List of abbreviations used in the thesis.

2 Structure and Function of the Axon

Axon

The axon is a specialized, elongated projection of a neuron responsible for transmitting action potentials (AP) from the soma to target cells such as other neurons, muscles, or glands. Axons exhibit substantial diversity in diameter, length, and degree of myelination, all of which critically influence their conduction properties. This thesis focuses on unmyelinated axons, which support continuous AP propagation along the membrane. These axons serve as valuable models for investigating the intrinsic electrical behavior of neuronal membranes and the kinetics of ion channels [6] (see Figure 1).

An axon originates at the axon initial segment (AIS), a highly specialized region typically 20–60 μm in length, characterized by a high density of voltage-gated sodium channels. This structural feature enables the AIS to serve as the primary site of AP initiation. Once initiated, the AP propagates along the axon via a combination of local circuit currents and the dynamic opening and closing of voltage-gated ion channels. This process is governed by biophysical parameters such as membrane resistance (R_m), membrane capacitance (C_m), axial resistance (R_a), and the electrochemical gradients of sodium and potassium ions [7].

Although once considered passive cables, axons are now recognized as active computational elements within neural circuits. They can perform analog-to-digital transformations, modulate spike timing and waveform through morphological features like branch points, varicosities, and diameter variations, and exhibit activity-dependent plasticity. Such plastic changes can alter both the morphological structure and the electrophysiological behavior of the axon over time [6] (see Figure 3). In Fig. 3, only the axon proper section of the full neuron illustration is used to represent the modeled axonal domain in this thesis.

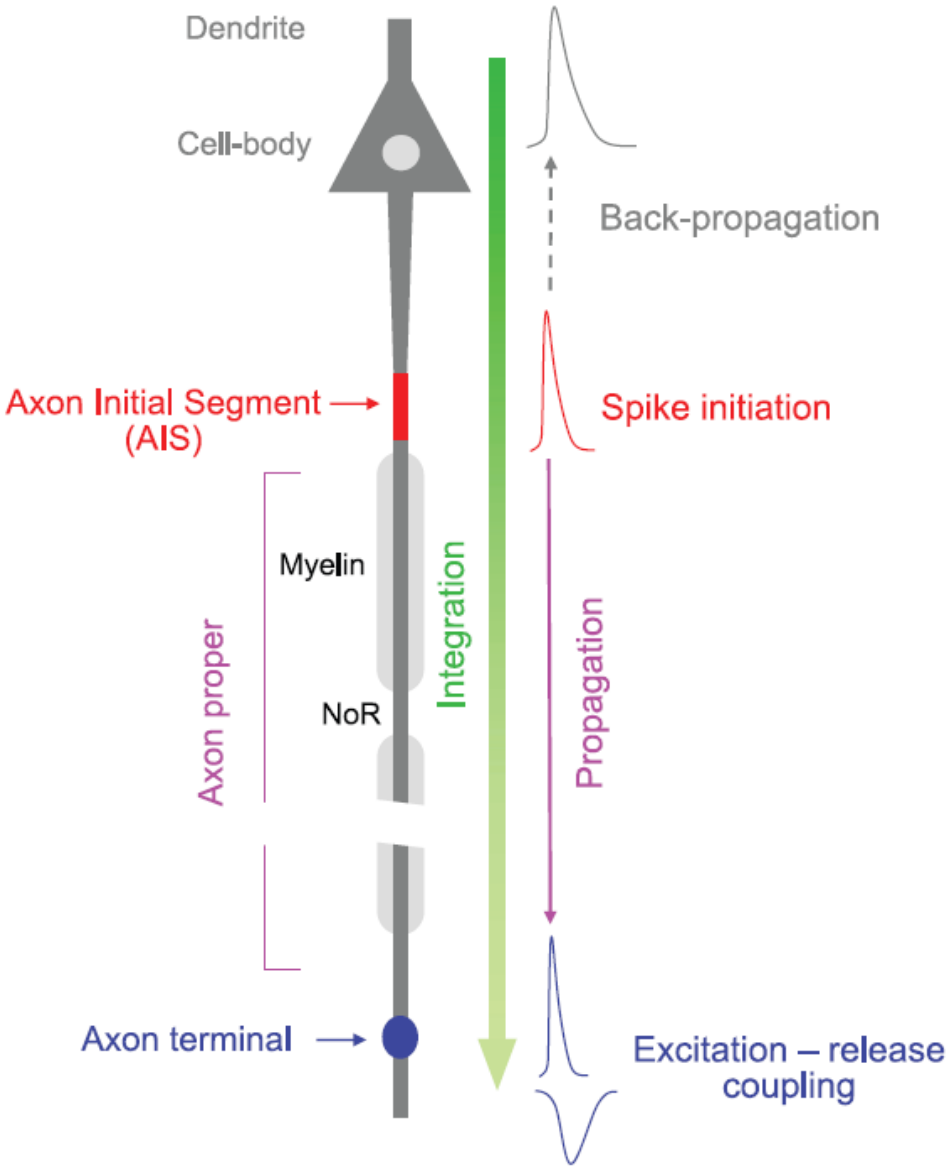

Figure 3: Summary of axonal functions. A pyramidal neuron is schematized with its different compartments. Four major functions of the axon are illustrated: (1) spike initiation at the axon initial segment (AIS), (2) spike propagation along the shaft, (3) excitation-release coupling at the terminal, and (4) integration of somatodendritic inputs that influence spike waveform and neurotransmitter release (green arrow) [6].

Functional Implications of Axon Morphology

Unmyelinated axons conduct signals via continuous propagation, wherein each segment of membrane must depolarize sequentially. This offeres opportunity to check the behaviour of the model in a relatively simple case when compared to myelinated axons which include additional geometry and processes [7, 9].

3 Theoretical Background

To model how an action potential (AP) travels along an axon, we begin with the classical cable equation like Hodgkin and Huxley (HH) [1]. This model treats the axon as an electrical cable composed of resistive and capacitive elements and describes how the membrane voltage evolves due to ionic currents and passive spread.

Hodgkin-Huxley cable equation is:

$$C_m \frac{\partial V}{\partial t} = \frac{1}{R_a} \frac{\partial^2 V}{\partial x^2} - I_{\text{ion}}(V, n, m, h), \tag{1}$$

this partial differential equation (PDE) expresses a balance between capacitive charging and ionic and axial currents. The terms are:

- $V(x,t)$: Membrane voltage at position x and time t [mV]
- C_m: Membrane capacitance per unit area [μF/cm^2]
- R_a: Axial resistance per unit length [Ω·cm]
- I_{ion}: Total transmembrane ionic current per unit area [μA/cm^2], which depends on:
  - g_K: Potassium channel conductance [m.mho/cm^2]
  - g_{Na}: Sodium channel conductance [m.mho/cm^2]
  - g_L: Leak channel conductance [m.mho/cm^2]
  - V_K, V_{Na}, V_L: Reversal potentials for K^+, Na^+, and leak channels [mV]
  - n, m, h: Gating variables representing voltage-dependent activation/inactivation

Lieberstein's Model

Lieberstein [2] extended the HH model [1] by starting from Maxwell's equations [4] [2]. This allowed the model to capture wave-like properties of voltage propagation in the axon, in contrast to the diffusion-type nature of the original HH cable equation. The ion currents are still treated using HH-type kinetics, but the cable is modeled as a distributed RLC circuit.

The following coupled partial differential equations (PDEs), as derived by Lieberstein [2].

$$\frac{\partial i_a}{\partial x} + i + \pi a^2 C_a \frac{\partial V}{\partial t} = 0 \tag{2}$$

$$\frac{\partial V}{\partial x} + r i_a + \frac{L}{\pi a^2} \frac{\partial i_a}{\partial t} = 0 \tag{3}$$

- $i_a(x,t)$: Axial current inside the axoplasm [μA]

- $i(x,t)$: Membrane current per unit length [μA/cm], given by:
  - $i = 2\pi a I_{\text{ion}}$
  - a: Axon radius [μm]
  - I_{ion}: Transmembrane ionic current per unit area [μA/cm^2]
- C_a: Capacitance of the axoplasm per unit volume [μF/cm^3]
- r: Longitudinal resistance per unit length [Ω/cm], computed as:
  - $r = \frac{R}{\pi a^2}$, where R is the axial resistance [Ω·cm]
- L: Inductance per unit length [mH·cm] [2, 3]

Derivation of the Combined Hyperbolic Cable Equation

Lieberstein's model [2] is based on the conservation of axial current and voltage drop along the axon, given by equations (2) and (3). By eliminating the internal current i_a between these two equations, one can derive a second-order partial differential equation (PDE) for the membrane voltage. The resulting equation takes the form:

$$\frac{\partial^2 V}{\partial x^2} - LC_a \frac{\partial^2 V}{\partial t^2} = RC_a \frac{\partial V}{\partial t} + \frac{2R}{a} I_{\text{ion}} + \frac{2L}{a} \frac{\partial I_{\text{ion}}}{\partial t} \tag{4}$$

this equation combines both the inductive and capacitive effects of the axoplasm and membrane. The left-hand side describes spatial and temporal propagation of the membrane voltage, while the right-hand side includes dissipative losses and nonlinear ionic source terms governed by the Hodgkin-Huxley model [1].

Ionic Currents and Gating Kinetics

The gating variables follow standard Hodgkin-Huxley dynamics [1], which describe the opening and closing of ion channels as voltage-dependent processes:

$$\frac{dn}{dt} = \alpha_n(V)(1-n) - \beta_n(V)n, \tag{5}$$

$$\frac{dm}{dt} = \alpha_m(V)(1-m) - \beta_m(V)m, \tag{6}$$

$$\frac{dh}{dt} = \alpha_h(V)(1-h) - \beta_h(V)h, \tag{7}$$

where each α and β is a voltage-dependent rate function:

- $\alpha_n(V), \beta_n(V)$: Rate constants for K^+ activation gate
- $\alpha_m(V), \beta_m(V)$: Rate constants for Na^+ activation gate
- $\alpha_h(V), \beta_h(V)$: Rate constants for Na^+ inactivation gate

The total ionic current is:

$$I_{\text{ion}} = g_K n^4 (V - V_K) + g_{Na} m^3 h (V - V_{Na}) + g_L (V - V_L) \tag{8}$$

Itemized current components:

- $g_K n^4 (V - V_K)$: Potassium current

- $g_{Na}m^3h(V - V_{Na})$: Sodium current
- $g_L(V - V_L)$: Leak current

each term depends on membrane voltage and gating variables, making the system nonlinear and highly sensitive to small changes in stimulus.

The rate constants α_i and β_i are taken the same as they are in the classical HH paper [1] for the squid giant axon at $6.3\ ^\circ\mathrm{C}$.

4 Numerical Methods

To solve the modified Hodgkin-Huxley model [1] in the Lieberstein framework [2], we implement a hybrid numerical approach combining spatial spectral accuracy with stable temporal integration. The system of partial differential equations (PDEs) derived from Maxwell's equations with added ionic kinetics is hyperbolic and nonlinear.

Pseudospectral Method in Space

Spatial derivatives are evaluated using a Fourier pseudospectral method, where variables are transformed into Fourier space using the Discrete Fourier Transform (DFT). The second spatial derivative is approximated as:

$$\frac{\partial^2 V}{\partial x^2} \approx \mathcal{F}^{-1}\left[-(k^2)\mathcal{F}[V(x,t)]\right], \tag{9}$$

where $\mathcal{F}$ and $\mathcal{F}^{-1}$ denote the Fourier and inverse Fourier transforms, respectively, and k is the spatial wave number. This method allows spectral convergence for smooth solutions and efficiently handles long axonal domains using Fast Fourier Transforms (FFT) [5].

Time Integration

Time integration is performed using an explicit Runge-Kutta method (RK45) via the `solve_ivp` routine in the SciPy Python library [10]. This method is well-suited for the stiff but moderately nonlinear nature of the Hodgkin-Huxley gating equations [1] combined with the inductive cable dynamics. This ensures flexibility and integration with scientific workflows.

Simulation Setup and Parameters

The following typical values [1], [2], [8] were used in simulations unless stated otherwise:

- Number of spatial nodes: $n = 2048$
- Time range: $t \in [0, 45]$ ms
- Axon radius: $a = 1$ μm
- Membrane capacitance: $C_m = 1$ μF/cm^2
- Axoplasmic capacitance: $C_a = 0.1$ μF/cm^3
- Axial resistance: $R = 32$ Ω·cm

- Inductance: $L = 40$ mH·cm

HH ionic parameters match the original squid axon setup: $g_{Na} = 120$, $g_K = 36$, $g_L = 0.3$ m.mho/cm^2, with initial gating values $n_0 = 0.318$, $m_0 = 0.052$, $h_0 = 0.596$ [1].

Mathematical Formulation of the System

The full system of equations used in this thesis originates from equations (2) and (3) introduced by Lieberstein [2], combined with Hodgkin-Huxley-type gating kinetics for ion channels [1]. These equations describe the axial current balance and voltage drop across an unmyelinated axon segment, with additional terms accounting for inductance and axoplasmic capacitance.

To simulate the voltage and current dynamics numerically, the model is reformulated as a system of first-order ordinary differential equations (ODEs) in time. Spatial derivatives are approximated using a Fourier pseudospectral method. The resulting system is:

$$\frac{\partial V}{\partial t} = \frac{-\partial i_a/\partial x - I_{\text{ion}}(V,n,m,h)}{A_{\text{const}}} + F(t,x), \tag{10}$$

$$\frac{\partial i_a}{\partial t} = \frac{-\partial V/\partial x - r i_a}{B_{\text{const}}}, \tag{11}$$

$$\frac{dn}{dt} = \alpha_n(V)(1-n) - \beta_n(V)n, \tag{12}$$

$$\frac{dm}{dt} = \alpha_m(V)(1-m) - \beta_m(V)m, \tag{13}$$

$$\frac{dh}{dt} = \alpha_h(V)(1-h) - \beta_h(V)h. \tag{14}$$

The total ionic current I_{ion} is defined as:

$$I_{\text{ion}} = 2\pi a \left[g_K n^4 (V - V_K) + g_{Na} m^3 h (V - V_{Na}) + g_L (V - V_L) \right], \tag{15}$$

where g_K, g_{Na}, g_L are the maximal conductances, and V_K, V_{Na}, V_L are the reversal potentials for potassium, sodium, and leak channels, respectively.

The geometric and electrical constants used in the model are:

$$A_{\text{const}} = \pi a^2 C_a + 2\pi a C_m, \tag{16}$$

$$B_{\text{const}} = \frac{L}{\pi a^2}, \tag{17}$$

where C_m is the membrane capacitance per unit area, C_a is the axoplasmic capacitance per unit volume, L is the inductance per unit length, and a is the axon radius. The resistance per unit length is given by $r = \frac{R}{\pi a^2}$, with R being the axial resistance.

The function $F(t, x)$ represents any external voltage input applied to the membrane and is used to stimulate action potentials in the simulations.

Initial and Boundary Conditions

The initial conditions are defined as follows:

- $V(x, 0) = 0$ mV: the axon is initially at rest.
- $i_a(x, 0) = 0$: no initial axial current.
- $n(x, 0) = 0.318$, $m(x, 0) = 0.052$, $h(x, 0) = 0.596$: steady-state gating variables based on [1].

External excitation is applied via a time-dependent input current $F(t, x)$ (see Equation 18), with units of mV. Boundary conditions are periodic due to the use of the Fourier pseudospectral method:

$$V(0, t) = V(L_x, t), \quad \frac{\partial V}{\partial x}(0, t) = \frac{\partial V}{\partial x}(L_x, t)$$

5 Localized Stimulus and Action Potential Initiation

To initiate action potentials (APs) in the model, we introduce an external voltage, denoted $F(t, x)$, which is added to the voltage equation as a forcing term. This voltage perturbs the membrane at a specific location and time, effectively modeling an external excitation such as a synaptic input or electrode-induced pulse. The stimulus is defined as a spatially localized Gaussian pulse that is applied for a limited time window:

$$F(t,x) = \begin{cases} A \cdot \exp\left(-\dfrac{(x - L_x/2)^2}{2\sigma^2}\right), & t_1 \leq t < t_2 \\ 0, & \text{otherwise} \end{cases} \tag{18}$$

Here:

- A is the stimulus amplitude in units of mV,
- σ is the spatial standard deviation of the pulse (typically in cm here),
- t_1 and t_2 define the temporal window during which the stimulus is active,
- L_x is the total axonal domain length.

This form ensures the stimulus is both spatially and temporally localized.

It is important to clarify that the value of A often referred to as the stimulus amplitude does not directly clamp the membrane voltage to a specific value, such as $V = -50\,\text{mV}$. Instead, it influences the dynamics of the system by contributing to the rate of change of the voltage, $\frac{\partial V}{\partial t}$. This is conceptually similar to injecting a brief, localized external current into the axon, which initiates but does not control the subsequent evolution of the membrane potential.

As a result, the membrane potential evolves according to the full set of differential equations, which include contributions from axial currents, ionic channel kinetics, and membrane capacitance. The actual voltage attained at the stimulation site depends on the cumulative effect of the applied stimulus and the nonlinear feedback mechanisms of ion channel gating. This allows the model to naturally reproduce the threshold-dependent, all-or-nothing behavior of action potentials. The resulting voltage trace may show much larger or smaller excursions depending on whether the stimulation successfully initiates a regenerative depolarization.

Advantages and Considerations

This method provides a computationally efficient and physically accurate framework for simulating action potential propagation. The retention of the inductance term allows the system to support wave-like behaviors.

The spectral method is particularly suitable due to the smoothness of voltage profiles and the large domains required to model realistic propagation. Time discretization is stable within tested step sizes and accurately resolves the rapid gating dynamics.

6 Task Statement and Research Objectives

The central aim of this thesis is to investigate how action potentials (APs) propagate in unmyelinated axons when modeled with a Lieberstein-extended version of the Hodgkin-Huxley (HH) model. Unlike the classical HH model, which treats the axon as a resistive-capacitive (RC) cable, the Lieberstein model includes additional electrical components such as inductance and axoplasmic capacitance, transforming the system into a resistor-inductor-capacitor (RLC) circuit.

The key research questions explored in this thesis include:

- Solving the equations 10 to 17 numerically.
- Checking that the solutions satisfy behaviours needed for AP (threshold, annihilation, relaxation time)
- Checking how do some physical and electrical parameters affect the solutions.

To address these questions, we conduct a series of five numerical simulations:

1. **Simulation 1: Single Stimulus Propagation**
   Objective: Demonstrate bidirectional AP propagation initiated by a single localized stimulus.
   Parameters: Default model values; no parameter variation.
2. **Simulation 2: Dual Peak Stimulation**
   Objective: Explore nonlinear interactions between two propagating APs.
   Parameters: Two spatially separated stimuli of equal magnitude.
3. **Simulation 3: Threshold Behavior**
   Objective: Identify the minimum stimulus amplitude required to elicit a full AP.
   Parameters: Varying stimulus strengths.
4. **Simulation 4: Refractory Dynamics**
   Objective: Assess the axon's recovery following a stimulus by applying a second identical stimulus with varying delays.
   Parameters: Fixed stimulus amplitude; variable time delays.
5. **Simulation 5: Parametric Study**
   Objective: Evaluate how changes in axon geometry and passive properties affect AP propagation.
   Parameters:
   - Axon radius a: 0.5 to 1.5 μm,
   - Axial resistance R: 0.5 to 1.5 $\times$ base value,
   - Membrane capacitance C_m: 0.5 to 1.5 $\times$ base value.

These simulations form the basis for evaluating the performance and insights offered by the Lieberstein-extended HH model in capturing biologically relevant behaviors.

7 Simulation Results

In this section we go trough the results that we got after solving the Lieberstein extended Hodgkin-Huxley model [2] (see Equations 10 and 11)

7.1 Results for Simulation 1

7.1.1 Simulation 1 Task

The task for Simulation 1 was for it to demonstrate bidirectional AP propagation initiated by a single stimulus.

7.1.2 Simulation 1 Parameters

Table 2: Simulation 1: Base Model Parameters (see [1, 2, 8])

Parameter	Value
Axon radius (a)	1.0 μm
Membrane capacitance per unit area (C_m)	1.0 μF/cm^2
Axoplasmic capacitance per unit volume (C_a)	0.1 μF/cm^3
Axial resistance (R)	32 Ω·cm
Inductance per unit length (L)	40 mH·cm
Simulation domain length (L_x)	12.56 cm
Number of spatial nodes (n)	2048
Time window	0 to 45 ms
Stimulus strength	$-11\ mV$
Stimulus width (σ)	0.5 cm
Stimulus center	$x = L_x/2$
Stimulus time window	1 to 2 ms
Initial gating variables	$n_0 = 0.318$, $m_0 = 0.052$, $h_0 = 0.596$
g_{Na} (Na^+ conductance)	120 m.mho/cm^2
g_K (K^+ conductance)	36 m.mho/cm^2
g_L (leak conductance)	0.3 m.mho/cm^2
V_{Na} (Na^+ reversal)	-115 mV
V_K (K^+ reversal)	12 mV
V_L (leak reversal)	-10.613 mV

7.1.3 Simulation 1 Findings

The applied localized stimulus successfully generated an action potential (see Fig. 5) at the midpoint of the axon. The AP then propagated symmetrically in both directions along the axon (see Fig. 4 and 8), consistent with expected physiological behavior of unmyelinated fibers.

To further characterize the dynamics of action potential propagation observed in Simulation 1, the ionic currents and gating variables were analyzed at a representative location along the axon, corresponding to the red trace in Fig. 5. The ionic currents (Fig. 6) exhibit the classical profile described by the Hodgkin-Huxley model [1]. At the onset of the action potential, a rapid inward sodium current is generated by the activation of voltage-gated sodium channels, which drives the membrane depolarization. As the membrane potential peaks, the sodium current quickly diminishes due to channel inactivation, while the potassium current, which activates more slowly, begins to rise. This delayed, outward potassium current facilitates membrane re-polarization. The leak current remains relatively small and constant throughout the process, serving primarily to maintain the resting potential rather than to shape the transient action potential waveform.

The gating variables m, h, and n (Fig. 7) evolve in a voltage-dependent manner, consistent with the original Hodgkin-Huxley kinetics [1]. The activation variable m, which controls sodium channel opening, increases sharply during the depolarization phase. Simultaneously, the inactivation variable h decreases, thereby limiting the duration of the sodium current. The potassium activation variable n increases more gradually but remains elevated during the repolarization and hyperpolarization phases, allowing for sustained potassium efflux. These coordinated gating dynamics produce the all-or-nothing behavior and refractory properties characteristic of real neurons. The results confirm that the Lieberstein-extended Hodgkin-Huxley model [2] accurately captures the essential biophysical mechanisms underlying action potential generation and symmetric bidirectional propagation in unmyelinated axons.

7.1.4 Simulation 1 Figures

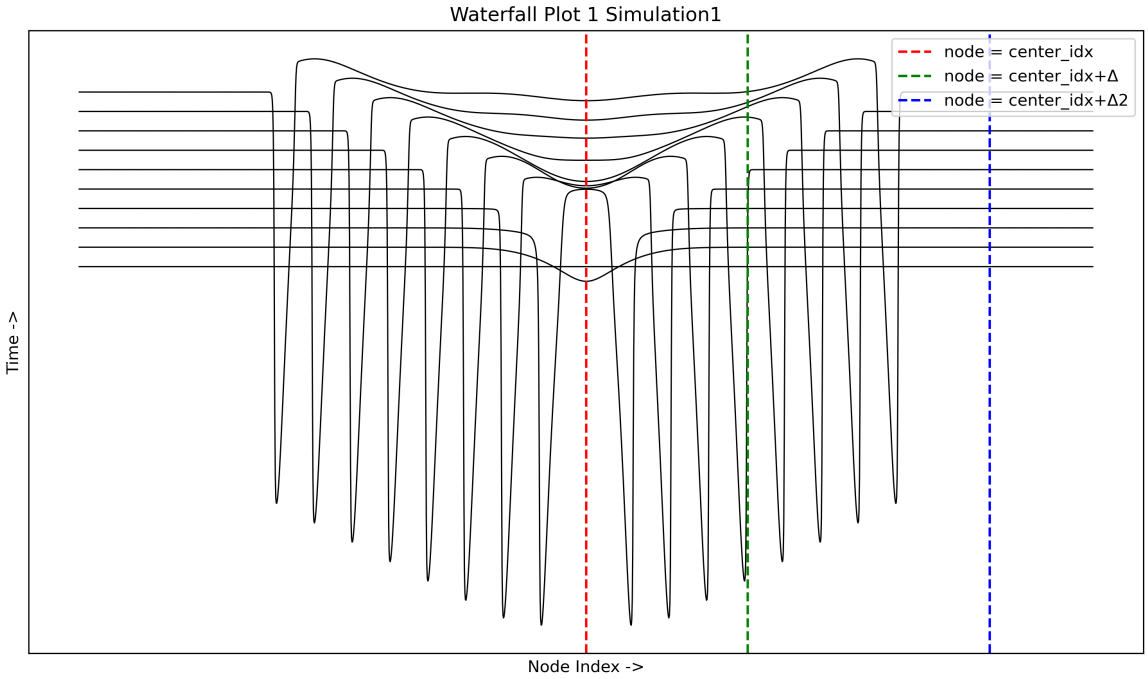

Figure 4: Waterfall plot where the nodes for the red, green, blue line for Fig. 5 are seen. Shows that the AP propagated symmetrically in both directions along the axon.

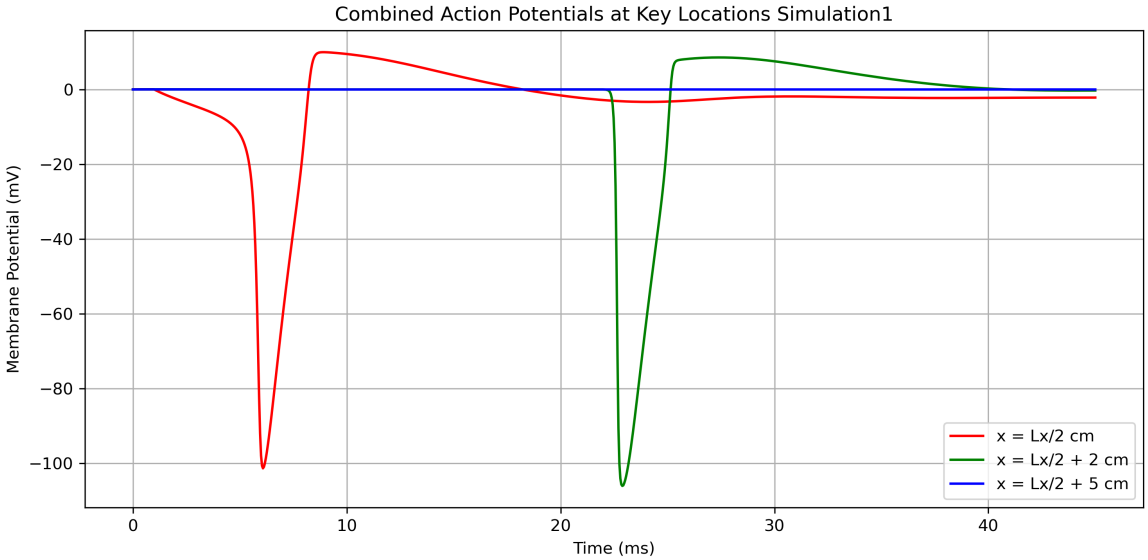

Figure 5: Combined Action Potentials (AP) at key locations in Simulation 1

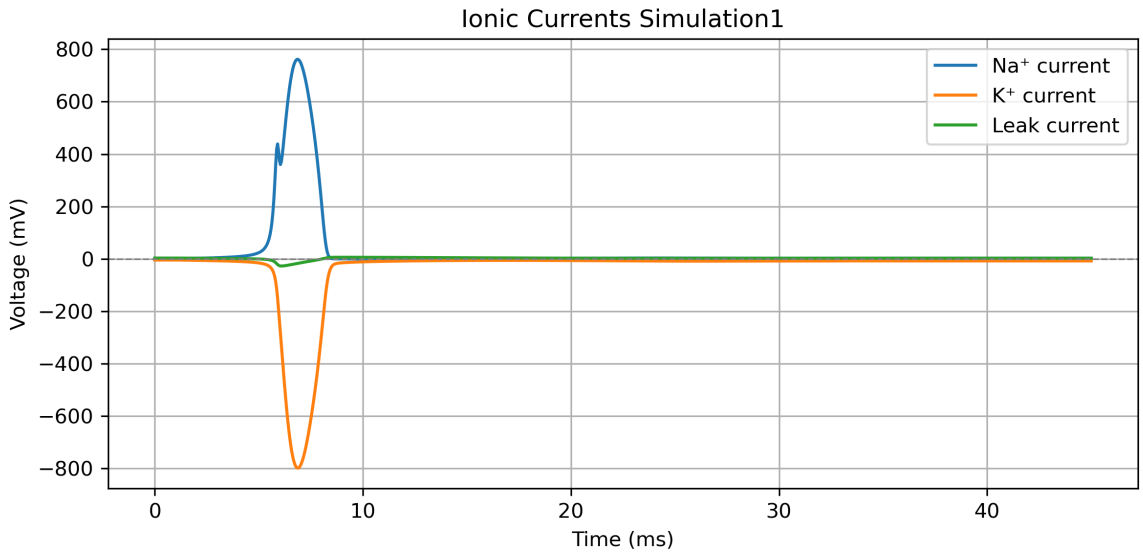

Figure 6: Ionic Currents for red line in Fig. 4

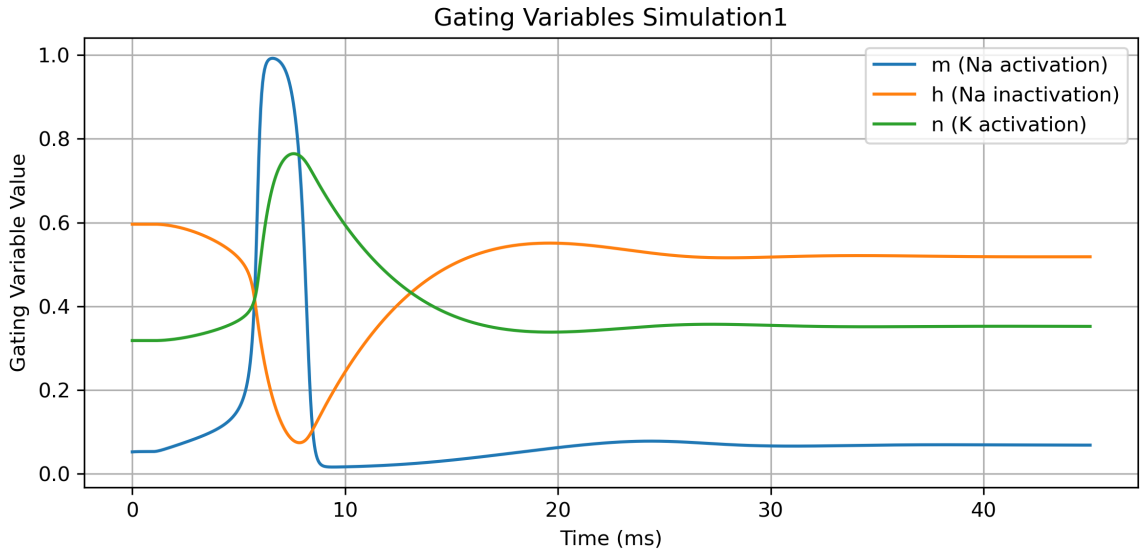

Figure 7: Gating Variables for red line in Fig. 4

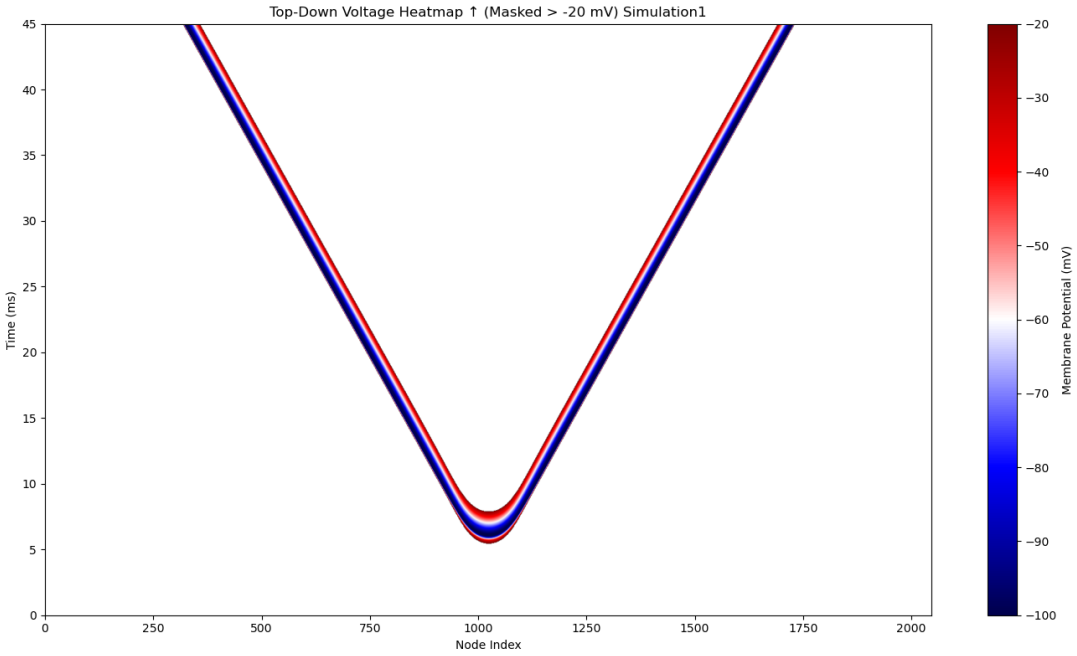

Figure 8: Heatmap plot where treshold is -20 mV. Shows that the AP propagated symmetrically in both directions along the axon.

7.2 Results for Simulation 2

7.2.1 Simulation 2 Task

The goal of Simulation 2 was to investigate nonlinear interactions between two action potentials initiated by dual localized stimuli placed at distinct spatial locations. Both stimuli had equal amplitude and duration.

7.2.2 Simulation 2 Parameters

Table 3: Simulation 2: Dual Stimulus Parameters and Base Model Settings (see [1, 2, 8])

Parameter	Value
Axon radius (a)	1.0 μm
Membrane capacitance per unit area (C_m)	1.0 μF/cm^2
Axoplasmic capacitance per unit volume (C_a)	0.1 μF/cm^3
Axial resistance (R)	32 Ω·cm
Inductance per unit length (L)	40 mH·cm
Simulation domain length (L_x)	12.56 cm
Number of spatial nodes (n)	2048
Time window	0 to 45 ms
Stimulus strength	$-20\ mV$
Stimulus width (σ)	0.5 cm
Stimulus centers	$x = L_x/2 \pm 2.5$ cm
Stimulus time window	1 to 45 ms
Initial gating variables	$n_0 = 0.318$, $m_0 = 0.052$, $h_0 = 0.596$
g_{Na} (Na^+ conductance)	120 m.mho/cm^2
g_K (K^+ conductance)	36 m.mho/cm^2
g_L (leak conductance)	0.3 m.mho/cm^2
V_{Na} (Na^+ reversal)	-115 mV
V_K (K^+ reversal)	12 mV
V_L (leak reversal)	-10.613 mV

7.2.3 Simulation 2 Findings

The AP, ionic currents and gating variables at the center of the axon is delayed by about 15 ms compared to the Fig. 5, Fig. 6 and, Fig. 7.

The 2 applied localized stimulus successfully generated an action potential (see Fig. 9) at the selected points of the axon (see Fig. 10). The AP then annihilated at the center point of the axon (see Fig. 10 and Fig.11), consistent with expected physiological behavior of unmyelinated fibers.

To further characterize the dynamics of action potential propagation observed in Simulation 1, the ionic currents and gating variables were analyzed at a representative location along the axon, corresponding to the red trace in Fig. 9.

In simulation 2, the ionic currents and gating variables behaved the same as in Fig. 6 and Fig. 7

7.2.4 Simulation 2 Figures

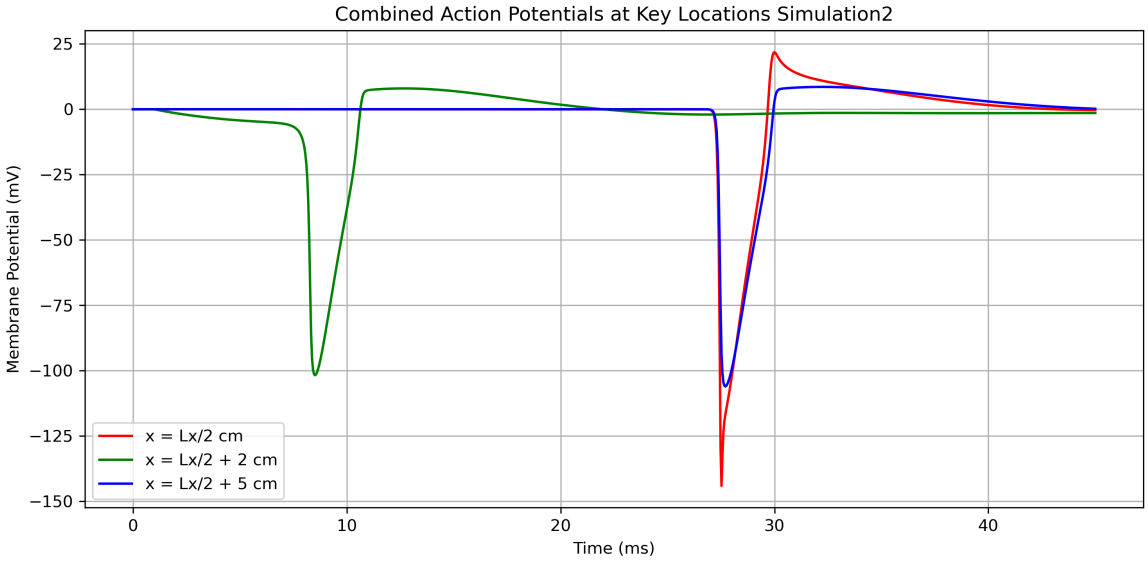

Figure 9: Combined Action Potentials (AP) at key locations in Simulation 2

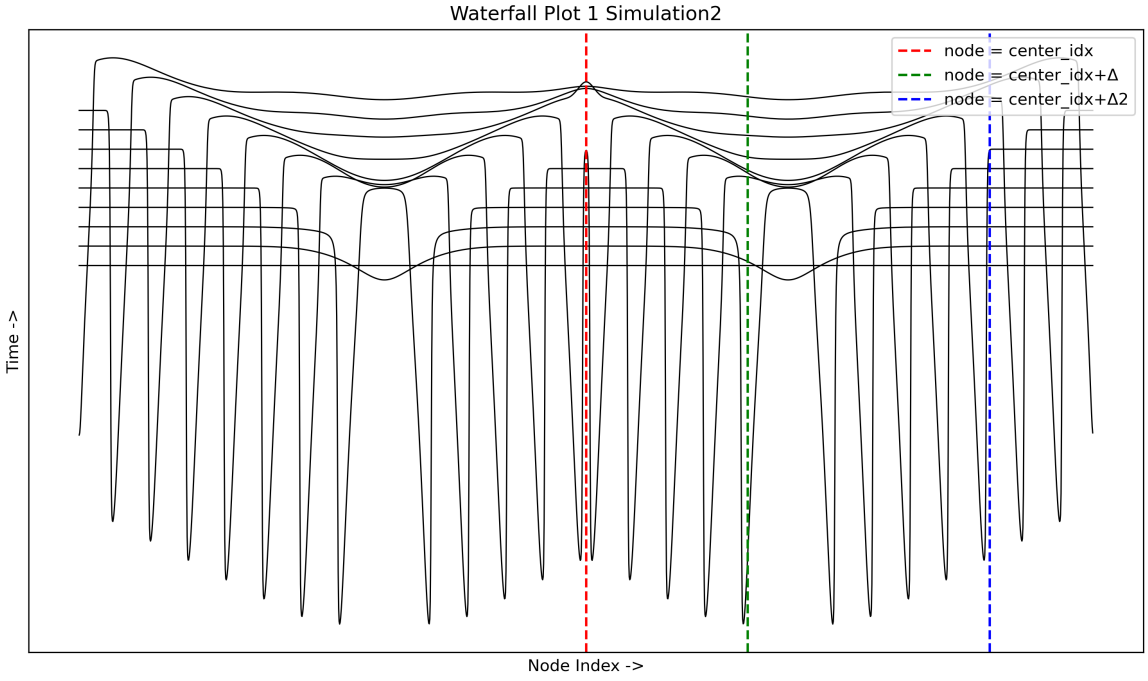

Figure 10: Waterfall plot where the nodes for the red, green, blue line for Fig. 9 are seen. Shows that the AP annihilated at the center from two spatially different but with the same membrane potential excitations.

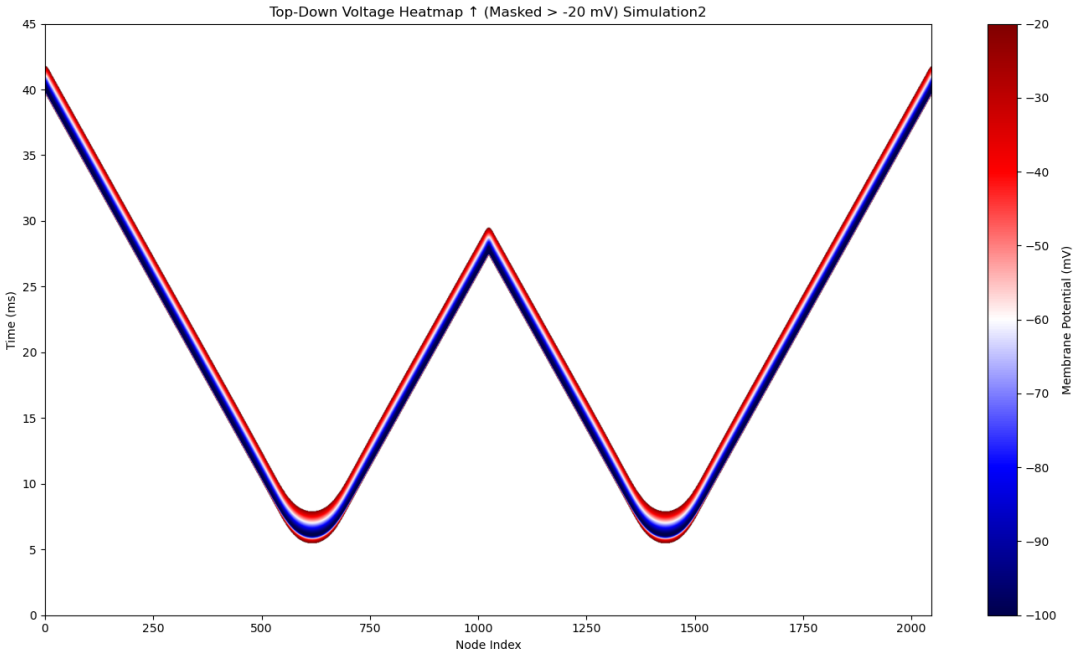

Figure 11: Heatmap plot where treshold is -20 mV. Shows that the AP annihilated at the center when two counter-propogatin AP.s collide head-on.

7.3 Results for Simulation 3

7.3.1 Simulation 3 Task

This simulation investigated the threshold behavior of the model by systematically varying stimulus amplitude from under threshold to above threshold values, while keeping other parameters constant.

7.3.2 Simulation 3 Parameters

Table 4: Simulation 3: Threshold Exploration Parameters and Base Model Settings (see [1, 2, 8])

Parameter	Value
Axon radius (a)	1.0 μm
Membrane capacitance per unit area (C_m)	1.0 μF/cm^2
Axoplasmic capacitance per unit volume (C_a)	0.1 μF/cm^3
Axial resistance (R)	32 Ω·cm
Inductance per unit length (L)	40 mH·cm
Simulation domain length (L_x)	12.56 cm
Number of spatial nodes (n)	2048
Time window	0 to 45 ms
Stimulus strength range	-101 to -1 mV (in steps of 1)
Stimulus width (σ)	0.5 cm
Stimulus centers	$x = L_x/2$
Stimulus time window	1 to 45 ms
Initial gating variables	$n_0 = 0.318$, $m_0 = 0.052$, $h_0 = 0.596$
g_{Na} (Na^+ conductance)	120 m.mho/cm^2
g_K (K^+ conductance)	36 m.mho/cm^2
g_L (leak conductance)	0.3 m.mho/cm^2
V_{Na} (Na^+ reversal)	-115 mV
V_K (K^+ reversal)	12 mV
V_L (leak reversal)	-10.613 mV

7.3.3 Simulation 3 Findings

The results showed a sharp transition between subthreshold and suprathreshold responses around a stimulus of -9 mV. Specifically:

- At an stimulation peak of about -8 mV (Fig. 12), no action potential was generated. The membrane depolarized slightly but quickly returned to resting potential without triggering sodium channel activation.
- At about -9 mV (Fig. 13), the model exhibited an excitable response that crossed the threshold and initiated a full AP, demonstrating the all-or-nothing behavior characteristic of real neurons.

These findings verify that the model successfully reproduces the threshold-dependent nature of neuronal excitability. The transition zone between failure (see Fig. 12) and success was narrow (see Fig. 13), indicating that the gating kinetics respond strongly and nonlinearly to small perturbations around the threshold. This aligns with biophysical observations of real axons and

reinforces the validity of the Lieberstein extension [2] for retaining adequate description of AP treshold phenomena.

7.3.4 Simulation 3 Figures

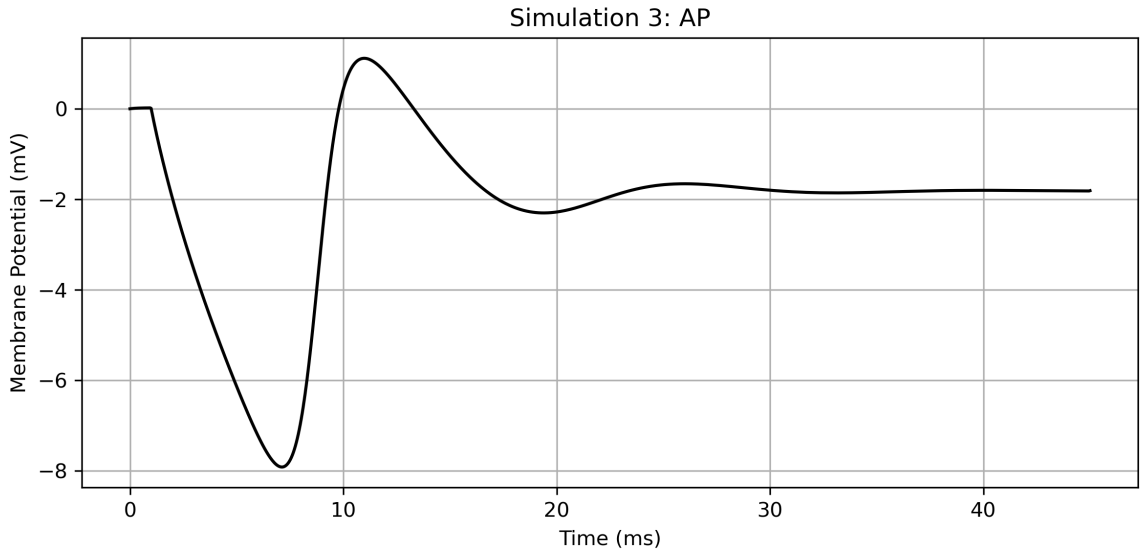

Figure 12: Action Potential at x=Lx/2 with a stimulation peak of about -8 mV, did not cross the treshold.

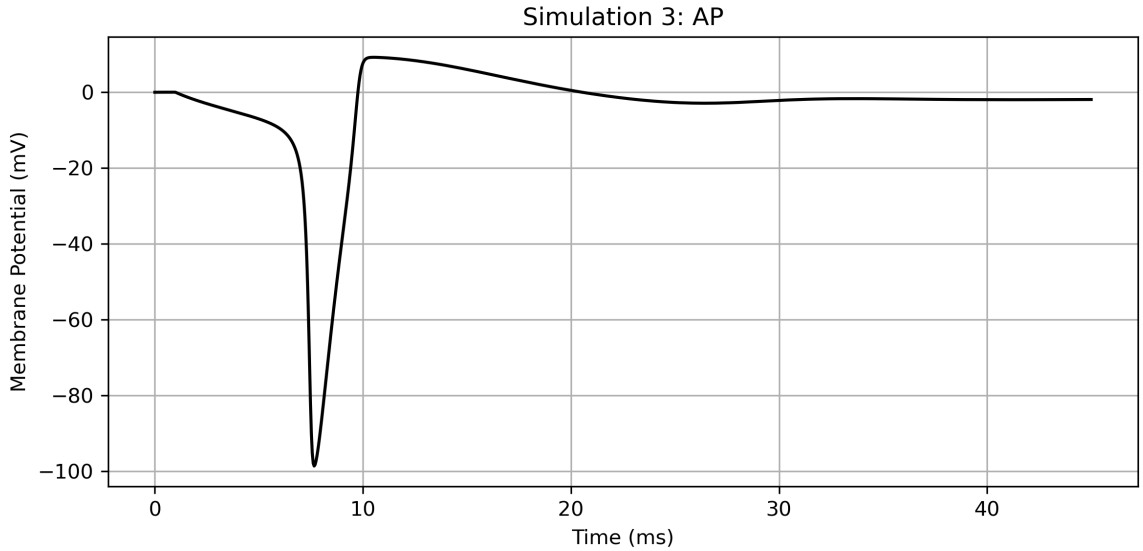

Figure 13: Action Potential at x=Lx/2 with a stimulation peak of about -9 mV, did cross the treshold

7.4 Results for Simulation 4

7.4.1 Simulation 4 Task

Simulation 4 investigated the refractory properties of the axon by applying a second identical stimulus pulse at varying delays following the first successful stimulus. The objective was to determine the minimal recovery time needed for the membrane to regain excitability sufficient to produce a second action potential (AP).

7.4.2 Simulation 4 Parameters

Table 5: Simulation 4: Refractory Period Investigation Parameters and Base Model Settings (see [1, 2, 8])

Parameter	Value
Axon radius (a)	1.0 μm
Membrane capacitance per unit area (C_m)	1.0 μF/cm^2
Axoplasmic capacitance per unit volume (C_a)	0.1 μF/cm^3
Axial resistance (R)	32 Ω·cm
Inductance per unit length (L)	40 mH·cm
Simulation domain length (L_x)	12.56 cm
Number of spatial nodes (n)	2048
Time window	0 to 45 ms
Stimulus strength	$-15\ mV$
Stimulus width (σ)	0.5 cm
Stimulus center (both pulses)	$x = L_x/2$
First stimulus time window	2 to 3 ms
Second stimulus time window	$[t_{\text{onset}},\ t_{\text{onset}} + 1]$ ms, $\quad t_{\text{onset}} \in [1,\ 50]$ ms
Initial gating variables	$n_0 = 0.318$, $m_0 = 0.052$, $h_0 = 0.596$
g_{Na} (Na$^+$ conductance)	120 m.mho/cm^2
g_K (K$^+$ conductance)	36 m.mho/cm^2
g_L (leak conductance)	0.3 m.mho/cm^2
V_{Na} (Na$^+$ reversal)	-115 mV
V_K (K$^+$ reversal)	12 mV
V_L (leak reversal)	-10.613 mV

7.4.3 Simulation 4 Findings

The results demonstrated that the ability of the second stimulus to evoke a full AP was highly dependent on the time delay between stimuli. When the second stimulus was applied too soon after the first (i.e., during the absolute refractory period) (see Fig. 14), it failed to generate any significant depolarization. As the delay increased, partial responses began to emerge, and at around a delay of 17 ms, a full second AP was reliably triggered (see Fig. 15)

This behavior matches the expected physiological properties of real neurons, where the inactivation of sodium channels and delayed recovery of potassium gating variables create a temporal window in which a second spike is suppressed. The membrane must return to a near-resting state before the gating variables allow another regenerative sodium influx.

The findings confirm that the Lieberstein-extended Hodgkin-Huxley model [2] successfully captures the time-dependent recovery process known as the refractory period.

7.4.4 Simulation 4 Figures

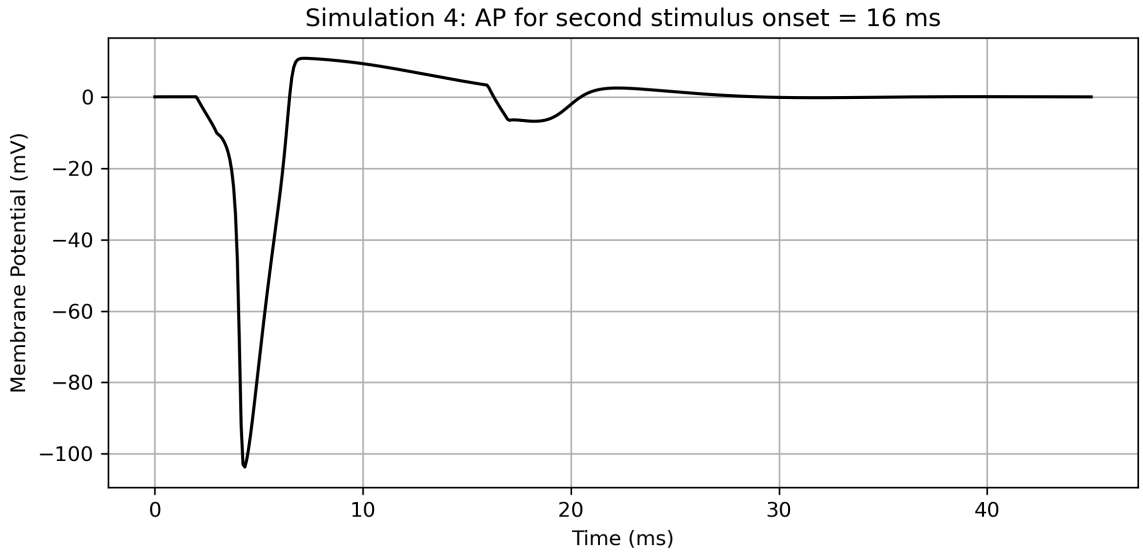

Figure 14: Membrane potential response at x=Lx/2 for Simulation 4 with second stimulus applied at 16 ms. The first action potential is triggered by the initial stimulus at 2 ms, while the second AP is unsuccessfully generated following a delay of 14 ms, indicating that the refractory period has not yet recovered.

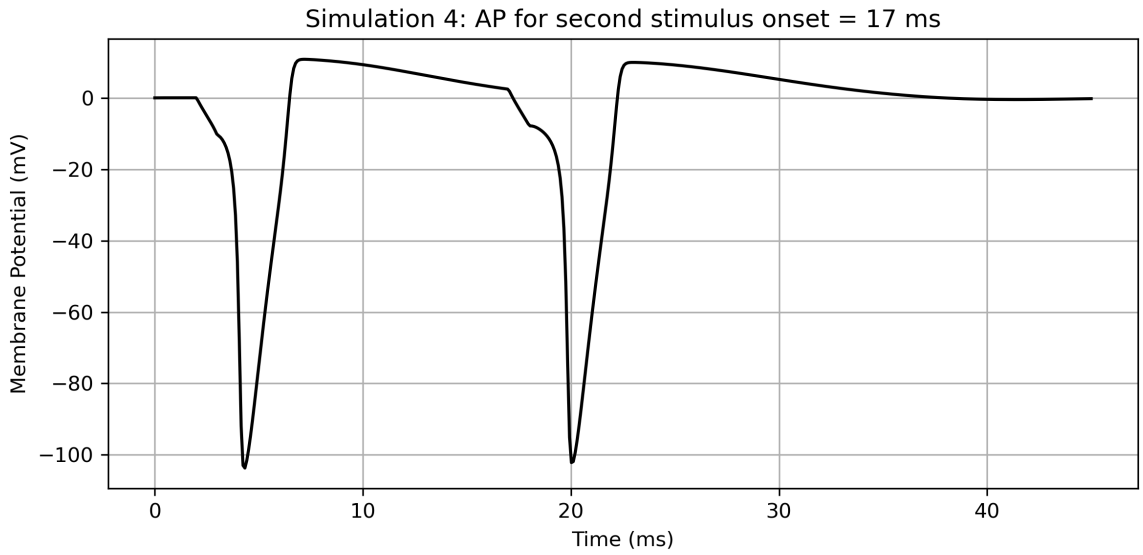

Figure 15: Membrane potential response at x=Lx/2 for Simulation 4 with second stimulus applied at 17 ms. The first action potential is triggered by the initial stimulus at 2 ms, while the second AP is successfully generated following a delay of 15 ms, indicating recovery from the refractory period.

7.5 Results for Simulation 5

7.5.1 Simulation 5 Task

Simulation 5 investigated how the geometric and electrical properties of the axon influence the amplitude of action potentials (APs). Specifically, the axon radius (a), axial resistance (R), and membrane capacitance per unit area (C_m) were varied independently and in combination across a range of values, and their effects were analyzed.

Parameters varied include:

- Axon radius a: from 0.5 to 1.5 $\times$ base value
- Axial resistance R: from 0.5 to 1.5 $\times$ base value
- Membrane capacitance C_m: from 0.5 to 1.5 $\times$ base value

7.5.2 Simulation 5 Parameters

Table 6: Simulation 5: Parametric Study of Geometric and Electrical Properties (see [1, 2, 8])

Parameter	Value / Range
Axon radius (a)	0.5 to 1.5 μm (in steps of 0.1)
Axial resistance (R)	16 to 48 Ω·cm (0.5x to 1.5x base)
Membrane capacitance (C_m)	0.5 to 1.5 μF/cm^2 (0.5x to 1.5x base)
Axoplasmic capacitance (C_a)	0.1 μF/cm^3 (constant)
Inductance per unit length (L)	40 mH·cm (constant)
Simulation domain length (L_x)	12.56 cm
Number of spatial nodes (n)	2048
Time window	0 to 45 ms
Stimulus amplitude	$-15\ mV$
Stimulus width (σ)	0.5 cm
Stimulus center	$x = L_x/2$
Stimulus time window	1 to 2 ms
Initial gating variables	$n_0 = 0.318$, $m_0 = 0.052$, $h_0 = 0.596$
g_{Na} (Na^+ conductance)	120 m.mho/cm^2
g_K (K^+ conductance)	36 m.mho/cm^2
g_L (leak conductance)	0.3 m.mho/cm^2
V_{Na} (Na^+ reversal)	-115 mV
V_K (K^+ reversal)	12 mV
V_L (leak reversal)	-10.613 mV

7.5.3 Simulation 5 Findings

The baseline configuration showed successful AP propagation with a characteristic shape and amplitude (Fig. 16). When C_m was increased to $1.5\times$ the base value, the resulting AP exhibited a lower peak voltage and broader waveform, suggesting greater capacitive loading slows the voltage response (Fig. 17). Conversely, reducing C_m to $0.5\times$ the base resulted in a sharper, higher-amplitude AP (Fig. 18).

Changes to axial resistance (R) had an inverse effect: increasing R to $1.5\times$ base value reduced peak AP amplitude and propagation efficiency (Fig. 19), while lowering R to $0.5\times$ enhanced AP strength and speed (Fig. 20). This is consistent with the expectation that higher axial resistance impedes longitudinal current flow, thus reducing AP efficacy.

Modifying axon radius (a) showed that larger axons ($1.5\times$ base) support higher amplitude and more robust APs (Fig. 21), while smaller axons ($0.5\times$ base) led to diminished signal propagation (Fig. 22). This reflects the relationship between radius and longitudinal resistance and capacitance in the cable model.

Overall, the results confirm that AP propagation is highly sensitive to the biophysical parameters

of the axon. Specifically:

- Larger radius and lower axial resistance support more efficient AP propagation.
- Higher membrane capacitance slows and dampens the voltage response.
- There exists a nonlinear interaction among the three parameters; simultaneous increases or decreases can either reinforce or counteract each other.

These findings demonstrate that tuning physical parameters of the axon model affects the shape and strength of action potentials, offering insights into how axonal geometry and membrane properties regulate signal transmission in biological systems.

7.5.4 Simulation 5 Figures

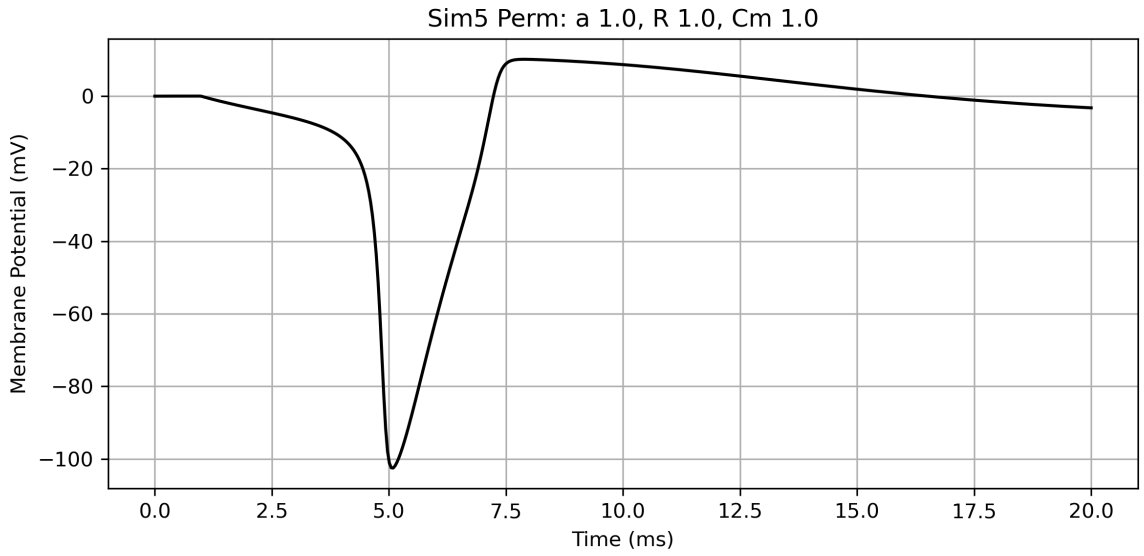

Figure 16: AP propagation with base values at x=Lx/2

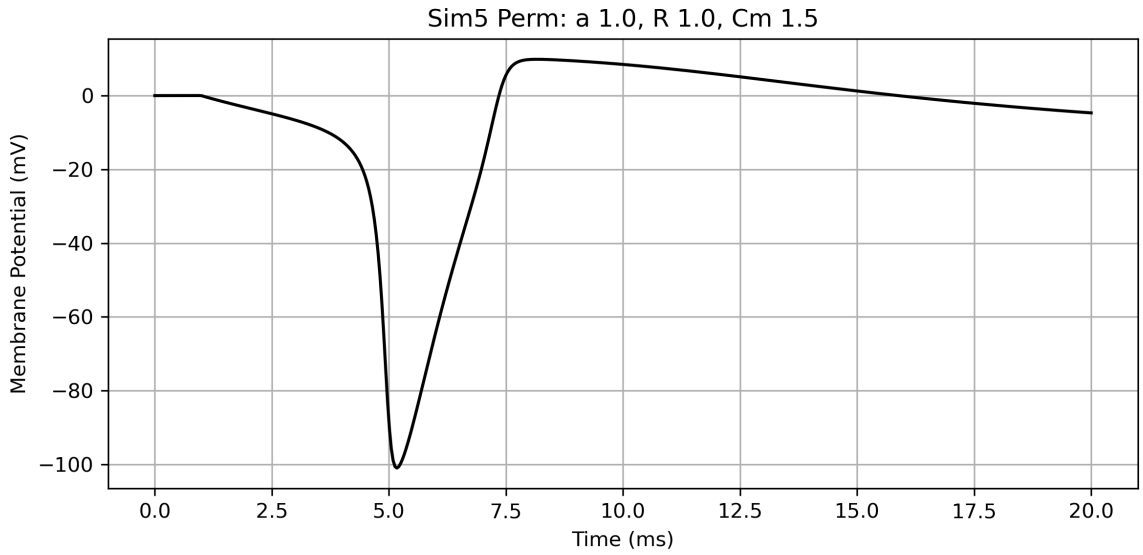

Figure 17: AP propagation with Cm base value $\times$ 1.5 at x=Lx/2

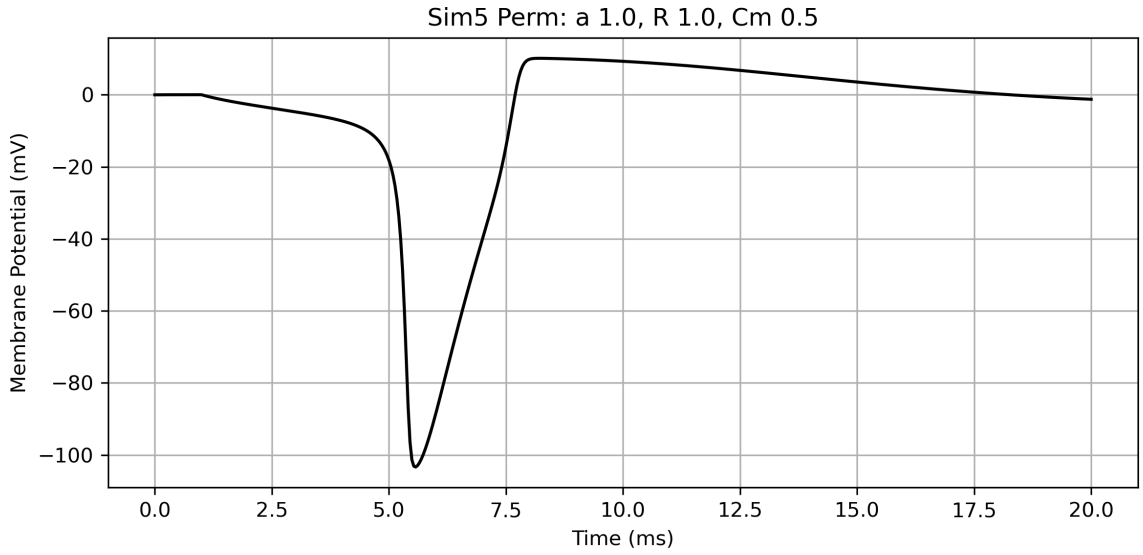

Figure 18: AP propagation with Cm base value $\times$ 0.5 at x=Lx/2

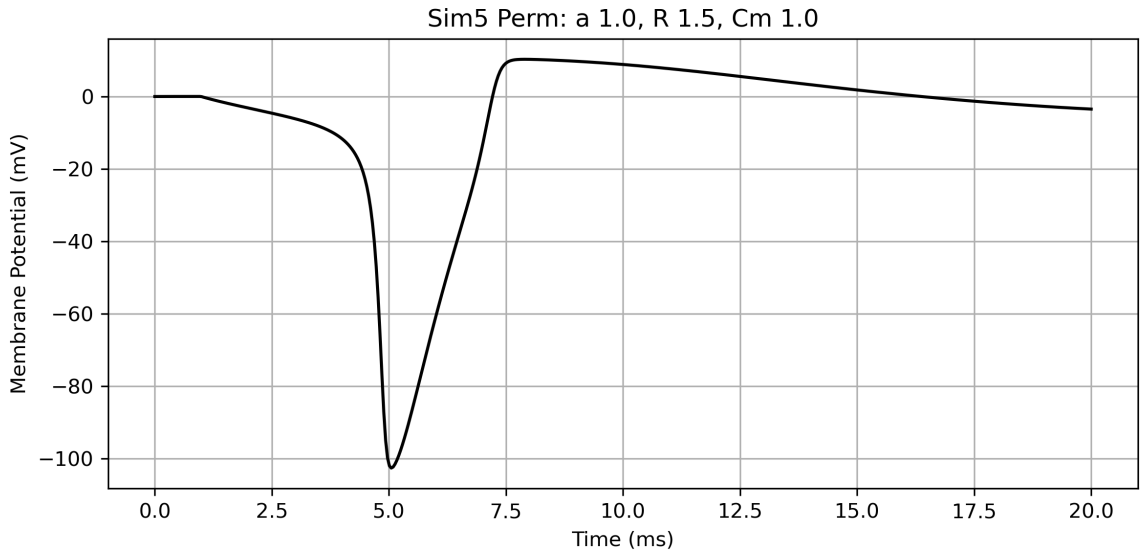

Figure 19: AP propagation with R base value $\times$ 1.5 at x=Lx/2

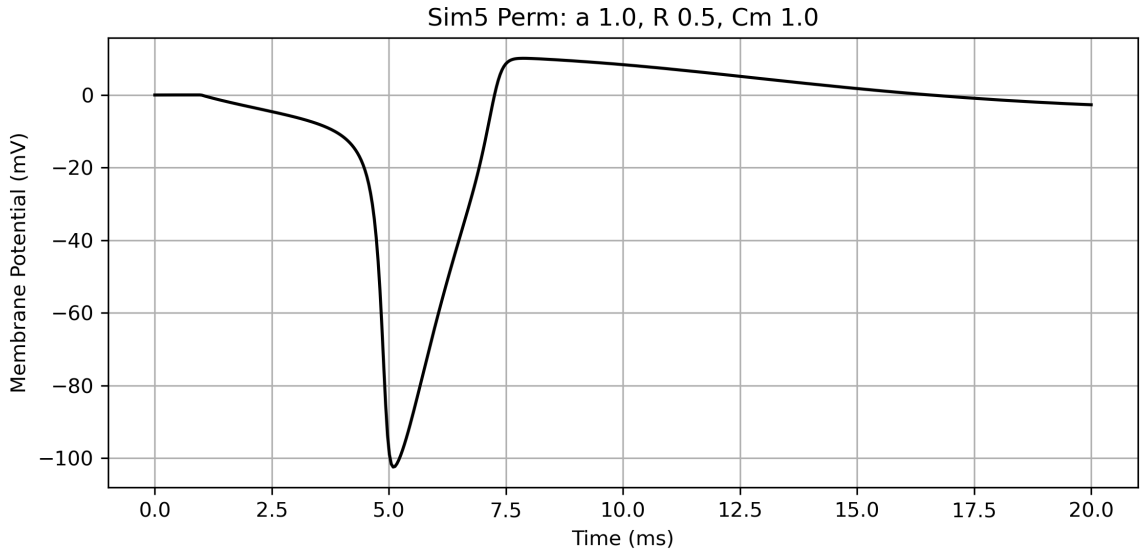

Figure 20: AP propagation with R base value $\times$ 0.5 at x=Lx/2

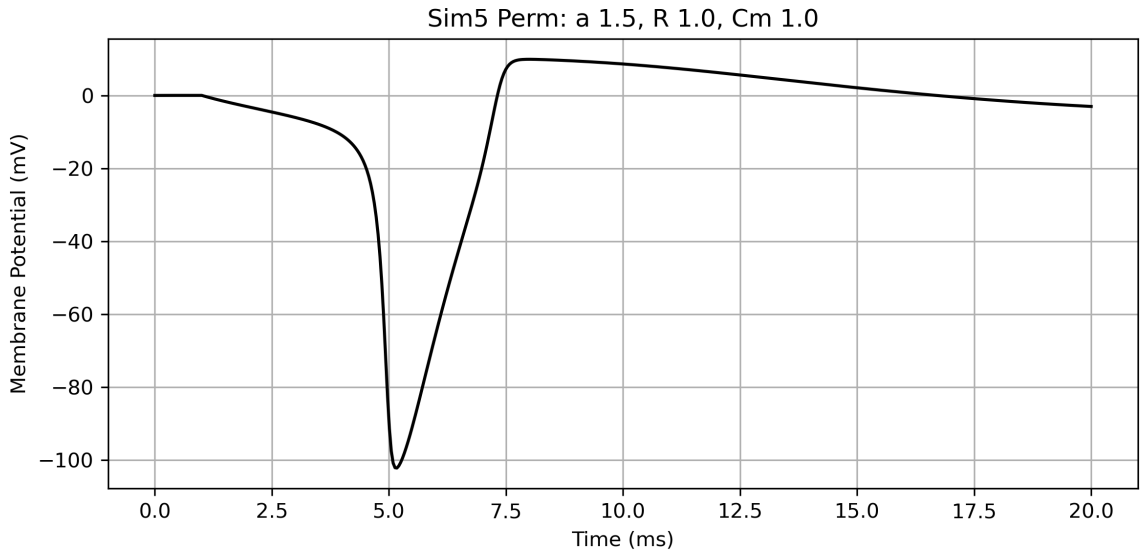

Figure 21: AP propagation with a base value $\times$ 1.5 at x=Lx/2

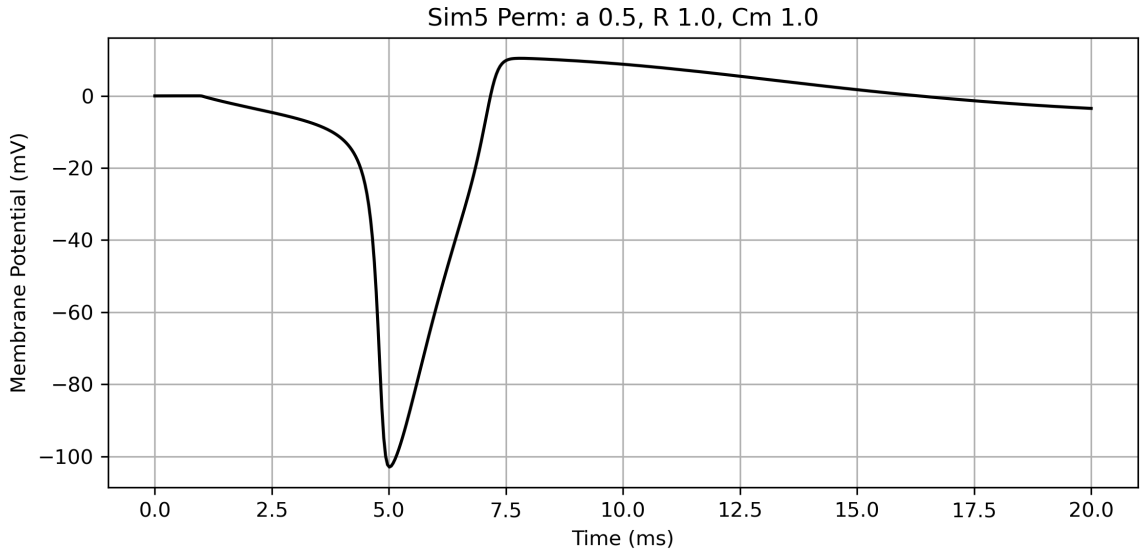

Figure 22: AP propagation with a base value $\times$ 0.5 at x=Lx/2

8 Summary

This thesis demonstrated how a modified version of the Hodgkin-Huxley (HH) model [1]—the Lieberstein-modified HH model [2]—can provide insight into how action potentials (APs) propagate along axons. While the original HH model offers a remarkably successful quantitative framework for describing ionic mechanisms underlying AP generation, it models the axon as a purely resistive-capacitive (RC) system. This simplification neglects inductive effects, which are typically small but can become significant in models emphasizing wave propagation. At the time, the focus was primarily on the local, diffusive aspects of signal initiation and shaping rather than on transmission speed or wave-like behaviors, hence inductance was not widely considered. Lieberstein's extension incorporates inductance and axoplasmic capacitance, enabling the description of voltage propagation as a damped wave, and offering a potentially richer framework for simulating signal transmission in long, unmyelinated axons.

Using Lieberstein extended Hodgkin-Huxley model, we simulated how action potentials behave in different situations. The first simulation showed that a single stimulus creates an action potential that travels in both directions. The signal had a clear rise and fall, and the simulation matched what we expect from nerve signals similar to Hodgkin-Huxley model [1].

In the second simulation, we applied two spatially separated stimuli that each initiated an action potential (AP). As the APs propagated toward each other, they met in the middle of the axon. Due to the refractory properties of the axonal membrane, where recently activated regions temporarily cannot support another AP, the two wavefronts did not pass through one another. Instead, they were annihilated upon collision, a well-documented behavior in excitable media. This result confirms that unmyelinated axons do not support overlapping signals traveling in opposite directions and highlights the unidirectional nature of AP propagation enforced by refractoriness.

In the third simulation, we changed the strength of the stimulus to find the minimum needed to trigger an action potential. This helped us understand the "threshold" for firing a signal. If the stimulus was too weak, the neuron stayed quiet. If it was strong enough, the signal was always the same shape and size, which reflects the all-or-nothing nature of real neurons.

The fourth simulation explored the refractory period more carefully. We applied two identical stimuli but changed the time delay between them. If the second stimulus came too soon, it failed to generate a signal. As we increased the delay, the neuron recovered and was able to fire again. This matches how real neurons behave and shows how they space out signals over time.

The fifth simulation demonstrated the influence of axonal geometry and electrical properties on the behavior of action potentials (APs). By systematically varying the axon radius (a), axial resistance (R), and membrane capacitance per unit area (C_m), the model demonstrated that these parameters collectively shape the amplitude, duration, and robustness of AP propagation.

We used efficient numerical methods to run these simulations, meaning Fourier transform for space and Runge-Kutta method for time. This allowed us to model long axons and fine details of

how voltage changes over time.

In summary this thesis demonstrates the influence of the previously noted parameters on the dynamics of solutions of the Lieberstein model and checks that the model behaves as expected for an AP (annihilation, threshold, refractory period).

In the future, this model could be extended to study more complex types of neurons, like those with myelin (insulation), and to look at how energy is used during signaling. It could also be connected to larger brain models to see how small changes at the single neuron level affect brain-wide communication.

References

[1] Hodgkin, A. L., and Huxley, A. F. (1952). A quantitative description of membrane current and its application to conduction and excitation in nerve. *The Journal of Physiology*, 117(4), 500–544.

[2] Lieberstein, H. (1967). On the Hodgkin-Huxley partial differential equation. *Mathematical Biosciences*, 1(3–4), 315–327.

[3] Lieberstein, H. M., & Mahrous, M. A. (1970). A source of large inductance and concentrated moving magnetic fields on axons. *Mathematical Biosciences*, 7, 41–60.

[4] Lucht, P. (2014). Transmission Lines and Maxwell's Equations. Rimrock Digital Technology. Retrieved from `https://www.researchgate.net/publication/276027908_Transmission_Lines_and_Maxwell%27s_Equations`

[5] Salupere, A. (2009). The pseudospectral method and discrete spectral analysis. In E. Quak & T. Soomere (Eds.), Applied Wave Mathematics (pp. 301–334). Springer. https://doi.org/10.1007/978-3-642-00585-5

[6] Debanne, D., Campanac, E., Bialowas, A., Carlier, E., & Alcaraz, G. (2011). Axon physiology. *Physiological Reviews*, 91(2), 555–602.

[7] Purves, D., Augustine, G. J., Fitzpatrick, D., et al. (2018). *Neuroscience* (6th ed.). Oxford University Press.

[8] Tamm, K., Peets, T., & Engelbrecht, J. (2023). The modelling of the action potentials in myelinated nerve fibres. `https://arxiv.org/abs/2406.18590`

[9] Sanders, F. K. (1948). The thickness of the myelin sheaths of normal and regenerating peripheral nerve fibres. *Philosophical Transactions of the Royal Society of London. Series B, Biological Sciences*, 135(323), 323–356.

[10] Virtanen, P., Gommers, R., Oliphant, T. E., et al. (2020). SciPy 1.0: Fundamental algorithms for scientific computing in Python. *Nature Methods*, 17, 261–272.

[11] By Thomas Splettstoesser (www.scistyle.com) - Own work, CC BY-SA 4.0, `https://commons.wikimedia.org/w/index.php?curid=41349083`

[12] By BruceBlaus - Own work, CC BY 3.0, `https://commons.wikimedia.org/w/index.php?curid=28761830`

Annex
to Rector's directive No 1-8/17 of 7 April 2020

Non-exclusive licence for reproduction and publication of a graduation thesis[1]

I Raigo Milvaste

1. grant Tallinn University of Technology free licence (non-exclusive licence) for my thesis Modeling Action Potential Propagation in Unmyelinated Axons,

supervised by Kert Tamm and Tanel Peets,

1.1 to be reproduced for the purposes of preservation and electronic publication of the graduation thesis, incl. to be entered in the digital collection of the library of Tallinn University of Technology until expiry of the term of copyright;

1.2 to be published via the web of Tallinn University of Technology, incl. to be entered in the digital collection of the library of Tallinn University of Technology until expiry of the term of copyright.

2. I am aware that the author also retains the rights specified in clause 1 of the non-exclusive licence.

3. I confirm that granting the non-exclusive licence does not infringe other persons' intellectual property rights, the rights arising from the Personal Data Protection Act or rights arising from other legislation.

---

23. 05. 2025

[1] *The non-exclusive licence is not valid during the validity of access restriction indicated in the student's application for restriction on access to the graduation thesis that has been signed by the school's dean, except in case of the university's right to reproduce the thesis for preservation purposes only. If a graduation thesis is based on the joint creative activity of two or more persons and the co-author(s) has/have not granted, by the set deadline, the student defending his/her graduation thesis consent to reproduce and publish the graduation thesis in compliance with clauses 1.1 and 1.2 of the non-exclusive licence, the non-exclusive license shall not be valid for the period.*